

Sodium in the Atmospheres of Thick-Disk Red Giants

Yu. V. Pakhomov¹

¹*Institute of Astronomy, Russian Academy of Sciences,
Pyatnitskaya ul. 48, Moscow, 109017 Russia, pakhomov@inasan.ru*

The parameters and elemental abundances of atmospheres for ten thick-disk red giants was determined from high-resolution spectra by the method of model stellar atmospheres. The results of a comparative analysis of the [Na/Fe] abundances in the atmospheres of the investigated stars and thin disk red giants are presented. Sodium in the atmospheres of thick-disk red giants is shown to have no overabundances typical of thin-disk red giants.

Keywords: stellar spectroscopy, stellar atmospheres, red giants, stellar evolution, kinematics, Galactic chemical evolution.

PACS: 97.10.Cv, 97.10.Ex, 97.10.Ri, 97.10.Tk, 97.20.Li, 98.35.Bd, 98.35.Df, 98.35.Pr

INTRODUCTION

The abundances of chemical elements in the atmospheres of stars are known to change in the course of their evolution. When investigating the chemical composition of giants, the first to be detected were the CNO abundance anomalies compared to the chemical composition of dwarf stars (see, e.g., [27, 28, 31, 44]). The observed sodium overabundance in the atmosphere of the red giant ϵ Vir was first mentioned in 1963 [19]. Subsequently, sodium overabundances were detected in red giants of the Hyades open cluster [29]. In another paper [30], the same authors found several giants with a [Na/Fe] overabundance and may have been the first to point out a systematic difference in sodium abundance between red giants and dwarfs. They hypothesized that sodium might be synthesized in some red giants. Slightly later, in 1970 [20] noted that the [Na/Fe] abundance increases with temperature parameter $\theta=5040/T_{\text{eff}}$. In other words, the [Na/Fe] abundance in cooler stars turned out to be, on average, higher, while giants are in the majority among these stars, i.e., the sodium abundance difference between dwarfs and giants is also noticeable, although the authors did not reach this conclusion.

[10] were the first to describe the dependence of the [Na/Fe] overabundances in the atmospheres of normal red giants on surface gravity. This dependence turned out to be similar to that discovered previously for supergiants [12, 13]. It was explained by the hypothesis that sodium could be produced in the $^{22}\text{Ne}(p,\gamma)^{23}\text{Na}$ reaction entering the neon-sodium cycle of hydrogen burning in the cores of main sequence stars and could then be brought from deep layers into the stellar atmosphere through developing convection as the star evolves from the main sequence to the red giant branch [14]. The calculations performed by [22, 23] confirmed the validity of this hypothesis. Further studies revealed [Na/Fe] overabundances in the atmospheres of various classes of red giants: moderate and classical barium stars [6, 15], super-metal rich stars [42]. A database of characteristics for red giants was created from the accumulated material at the Institute of Astronomy, the Russian Academy of Sciences. Our studies using the database revealed several

stars with a [Na/Fe] underabundance relative to the observed dependence on surface gravity [7, 42]. A comparative analysis showed that these stars are distinguished by slightly higher space velocities. To confirm this conclusion, we investigated the chemical composition of red giants with high Galactic velocities [39] and pointed out that 12 of the 14 investigated stars also have a [Na/Fe] underabundance.

There exist quite a few works devoted to the abundance analysis of Galactic thin- and thick-disk stars. These works are based on spectroscopic observations of dwarfs, because their atmospheric elemental abundances undergo no changes as they evolve on the main sequence. Besides, in comparison with giants, dwarfs form a larger group and their continuum spectrum exhibits a smaller number of spectral lines, which increases the accuracy of abundance determinations. Therefore, there are comparatively few works devoted to thick-disk giants. There are even fewer studies of sodium in thick-disk giants (see, e.g., [3, 45]). In these papers, the dependences of the [Na/Fe] abundance on mass and metallicity are discussed, but such an important factor as the evolutionary status is overlooked. Since the sodium abundances in stellar atmospheres do not appear instantaneously but gradually increase since the first deep mixing, the evolutionary stage of the star should be taken into account. In this paper, we perform a comparative analysis of the [Na/Fe] abundance in the atmospheres of thin and thick-disk red giants as a function of their metallicity and surface gravity, which changes during the lifetime of a star. Thus, investigating the changes in the atmospheric sodium abundance of red giants is necessary for understanding the stellar evolution, while the detected sodium underabundance in thick disk giants requires a further study.

OBSERVATIONS

Selection of Stars

We selected the objects for our observations from the Hipparcos catalogue [47] by analyzing the Galactic velocities (UVW) calculated using reduced Hippar-

TABLE I: The list of investigated stars with the membership probabilities (p) in the Galactic thin and thick disks

N	HD	α_{2000}	δ_{2000}	m_V	SpType	$p, \%$	
		h:m:s	° : ' : "			thin disk	thick disk
1	249	00 07 22.56332	+26 27 02.1686	7.33	K1IV	0	99
2	6555	01 06 38.62642	+23 13 57.4834	7.95	K0III-IV	15	84
3	10057	01 38 19.91771	+02 35 09.8395	6.92	K0	1	97
4	24758	03 59 17.62739	+57 59 13.6255	8.67	K0III	0	99
5	37171	05 37 04.38211	+11 02 06.0293	6.00	K5III	0	99
6	80966	09 23 50.43122	+34 32 53.3986	7.17	K0	0	99
7	180682	19 15 43.69429	+40 21 35.7242	6.96	K0	0	99
8	203344	21 21 04.39426	+23 51 21.4872	5.57	K1III	0	99
9	211683	22 18 37.60252	+10 21 18.7937	7.73	K2	20	79
10	212074	22 21 27.94691	+14 53 49.6214	7.64	K1IV	3	96

TABLE II: Kinematic parameters of the investigated stars: the Galactic velocity vector components (U, V, W) and Galactic orbital elements

N	HD	U	V	W	R_{min}	R_{max}	Z_{max}	e
		$km s^{-1}$						
1	249	45.4±3.1	-55.5± 5.2	-78.6± 5.3	6.00±0.14	8.93±0.04	1.46±0.09	0.20±0.01
2	6555	-25.0±4.0	-12.1± 3.0	-68.3± 5.8	7.98±0.06	10.04±0.13	1.21±0.10	0.11±0.01
3	10057	3.6±7.1	-46.8± 7.0	55.6± 1.3	6.90±0.24	8.70±0.02	1.38±0.02	0.12±0.02
4	24758	-123.7±4.3	-23.8± 7.9	-84.2±13.8	5.98±0.12	14.64±0.38	2.36±0.41	0.42±0.01
5	37171	-113.1±0.8	-19.0±10.4	65.2± 9.5	6.15±0.15	14.42±0.42	2.18±0.25	0.40±0.00
6	80966	-23.4±14.0	-105.4±23.8	75.5± 9.5	3.92±0.56	8.83±0.08	2.15±0.19	0.39±0.06
7	180682	-89.7±8.7	-11.6± 4.2	59.6± 5.7	6.72±0.10	12.70±0.31	1.70±0.13	0.31±0.02
8	203344	61.5±1.0	-102.4± 0.6	-70.1± 2.5	3.69±0.02	8.86±0.01	1.21±0.05	0.41±0.00
9	211683	-7.1±4.4	-20.2± 3.3	50.2± 5.7	8.12±0.09	8.75±0.11	1.06±0.08	0.04±0.01
10	212074	-6.2±3.0	-5.9± 5.5	61.5± 8.7	8.34±0.02	9.94±0.27	1.46±0.16	0.09±0.01

cos parallaxes and CORAVEL radial velocities [37]. The selection criteria were the (B-V) color indices and calculated surface gravities corresponding to red giants; the calculated Galactic velocities exceeding those typical of thin-disk stars (34.5, 22.5, 18.0) $km s^{-1}$ [24], with $W < 50 km s^{-1}$.

The list of program stars is presented in Table I, where their ordinal numbers, HD numbers, coordinates, V magnitudes, and spectral types are given. The last two columns in Table I provide the membership probabilities of the program stars in the Galactic thin and thick disks, whose kinematic characteristics were taken from [24]. The probabilities were calculated using formulas from [38]. It can be seen from the table that all stars can be assigned to thick-disk objects with a high probability.

Table II presents kinematic characteristics of the investigated stars. These include the Galactic velocity vector (U, V, W) relative to the Sun and Galactic orbital elements: the perigalactic distance R_{min} , the apogalactic distance R_{max} , the maximum orbital distance from the Galactic plane Z_{max} , the eccentricity e , and the inclination i . The distance to the Galactic center was assumed to be 8.5 kpc, while the necessary correction of the veloc-

ities for the solar motion, (+10.2, +14.9, +7.8) $km s^{-1}$, was taken from [24]. We calculated the orbital elements through numerical integration of the stellar motion by Everhart's 15th-order method using a three-component model Galactic potential [2]. The integration accuracy was controlled by the conservation of the necessary integrals of motion. For example, in ten orbital revolutions, the typical relative error was $\Delta h/h < 10^{-13}$ in angular momentum and $\Delta E/E < 10^{-8}$ in total energy. The errors in the space velocities ($\sigma U, \sigma V, \sigma W$) were calculated from the errors in the stellar proper motions, radial velocities, parallaxes and the errors in the solar velocity components relative to the local standard of rest. We calculated the errors in the Galactic orbital elements based on the model Galactic gravitational potential using the probable errors in the stellar space velocities. It can be seen from Table 2 that all stars have a maximum orbital distance from the Galactic plane $Z_{max} > 1000$ pc, which exceeds considerably the characteristic scale height for thin-disk objects, 90-325 pc ([25], [43], [21]). More than half of the investigated stars have orbits with eccentricities larger than 0.2. About half of the stars recede to a distance of more than 10 kpc from the Galactic center when moving in their orbits.

TABLE III: Parameters of atmosphere of the investigated stars, their masses, and interstellar extinctions

N	HD	T_{eff} K	$\lg g$	V_t $km\ s^{-1}$	[Fe/H]	Mass M_{\odot}	A_V m
1	249	4850	2.96	1.17	-0.15	1.5 ± 0.2	0
2	6555	4720	3.00	1.15	-0.09	1.2 ± 0.2	<0.1
3	10057	4130	1.70	1.35	-0.30	1.7 ± 0.3	0.3
4	24758	4680	2.75	1.15	0.11	1.4 ± 0.2	0
5	37171	4000	1.25	1.35	-0.55	1.1 ± 0.2	0.5
6	80966	4550	1.80	1.50	-1.01	1.2 ± 0.3	<0.1
7	180682	4330	1.90	1.40	-0.43	1.1 ± 0.2	0.3
8	203344	4770	2.75	1.30	-0.09	1.8 ± 0.2	0
9	211683	4450	1.80	1.35	-0.13	1.9 ± 0.3	0.3
10	212074	4700	2.55	1.30	0.05	2.3 ± 0.3	<0.1

Spectroscopic Observations

The spectroscopic observations of the selected stars were performed in 2010 with a two-band echelle spectrograph attached to a 2.16-m telescope at the Xing-long station of the National Astronomical Observatories of China (NAOC). The spectrograph operated in the red-band mode. The detector was a 2048x2048 CCD array on which 45 spectral orders were recorded. The in the range from 5500 to 9830 Å spectrograph resolution was $R = 40\,000$; the signal-to-noise ratio in the spectra was $S/N > 100$. The *echelle* package of the *MIDAS* software system was used for the preliminary spectroscopic data reduction, the search for and extraction of the spectral orders, the wavelength calibration using the spectrum of a thorium-argon lamp, and the spectrum normalization.

The equivalent widths of the selected spectral lines were measured in the EW code that I developed. The code is a set of modules written in Perl and C, the access to which is organized via a graphical user interface. The automatic equivalent width determination module is the main one in the code. It uses the nonlinear Levenberg-Marquardt algorithm from the PDL package. For each measured spectral line with wavelength λ_0 , the part of the spectrum $\lambda_0 \pm 10\lambda_0/R$ in which the spectral lines are searched for is cut out. An iterative deconvolution method is applied for a better line detection; it allows the blends to be separated. More or less significant lines can be identified by varying the number of iterations. Each spectral line is fitted by a Gaussian, which is a normal approximation for most of the lines with equivalent widths $< 100\text{ mÅ}$. The investigated part of the spectrum is fitted by the sum of Gaussians $F(\lambda) = \sum_{i=0}^k h_i * e^{-(\lambda_i - \lambda_0)^2 / \sigma_i^2}$, where h_i and σ_i are the and width of the i spectral line. We take the depth of the observed line as the initial approximation for h and $\sigma = \lambda_0/R$ for the width. The module operation result is a set of parameters of the Gaussians that best fit the observed spectrum. The parameters of the investigated spectral line are written in a file. In addition, information about the quality of the

fit and the degree of line blending is written. During its operation, the code displays a theoretical spectrum of atomic and molecular lines that provides an additional possibility for the selection of lines.

DETERMINATION OF STELLAR ATMOSPHERE PARAMETERS

We determined the stellar atmosphere parameters using a technique based on Kurucz's model atmospheres [16] and analysis of the relative abundances of iron-peak elements. The technique is described in detail in [10]) and allows the stellar atmosphere parameters for G-K giants to be determined with an accuracy of about 70-100 K for T_{eff} , 0.10-0.15 for $\lg g$, and 0.10-0.15 $km\ s^{-1}$ for V_t . For late-K giants, the accuracy can be lower due to the greater influence of blending by atomic and molecular lines. In this paper, when analyzing the relative abundances of iron-peak elements when determining the stellar atmosphere parameters, we disregarded titanium, because it is well known that the [Ti/Fe] abundance can be enhanced at low metallicities and for thick-disk stars [8]. Using the derived parameters (T_{eff} , $\lg g$, V_t), we computed the corresponding model stellar atmospheres with the ATLAS9 code [34].

Table III gives our estimates of the stellar atmosphere parameters (effective temperature T_{eff} , surface gravity $\lg g$, microturbulence V_t , and metallicity [Fe/H]), masses, and interstellar extinctions A_V . We determined the masses based on evolutionary tracks from [26] by taking into account the stellar metallicity. The interstellar extinctions were estimated from the color excess $E(B-V)$; the dereddened colors were calculated from calibrations [9] based on Kurucz's model stellar atmospheres. Based on the measured equivalent widths of the selected unblended spectral lines, we estimated the elemental abundances with the WIDTH9 code. These are presented in Table IV and Fig. 1, where the open circles and asterisks denote the abundances determined from the spectral lines of neutral and ionized atoms, respectively. The list of selected lines with their characteristics and equivalent widths is available in electronic form. The cobalt abundance was determined by taking into account the hyperfine splitting effect, which can be strong in the case of cool giants [11]. The abundance errors given in Table IV and marked by the bars in Fig. 1 were determined as the dispersion of the individual abundances calculated from individual spectral lines. As an example, the possible abundance errors associated with the determination of stellar atmosphere parameters are listed in Table V for two stars. Table V gives the number of lines used (N) and the changes in the abundance of each element when changing individual model parameters ($\Delta T_{\text{eff}} = +100\text{K}$, $\Delta \lg g = +0.10$, $\Delta V_t = +0.10\text{ km s}^{-1}$) and the total change in abundance Δ .

The sodium abundance was determined from the 6154Å and 6160 Å lines without any correction for non-

TABLE IV: Abundances of chemical elements in atmospheres of the studied stars

	HD 249		HD 6555		HD 10057		HD 24758		HD 37171		HD 80966		HD 180682		HD 203344		HD 211683		HD 212074	
	N	[X/H]	N	[X/H]	N	[X/H]	N	[X/H]	N	[X/H]	N	[X/H]	N	[X/H]	N	[X/H]	N	[X/H]	N	[X/H]
NaI	2	-0.23±0.04	2	-0.03±0.09	2	-0.26±0.08	2	0.33±0.07	1	-0.66	2	-1.22±0.02	2	-0.36±0.04	2	-0.03±0.11	2	-0.07±0.15	2	0.04±0.07
MgI	2	-0.03±0.02	2	0.17±0.04	2	-0.06±0.04	2	0.21±0.03	2	-0.29±0.08	2	-0.60±0.06	2	-0.12±0.04	2	0.16±0.01	2	0.08±0.05	2	0.26±0.05
AlI	2	0.06±0.02	2	0.20±0.01	2	0.05±0.09	2	0.20±0.01	2	-0.19±0.05	2	-0.72±0.02	2	-0.10±0.04	2	0.18±0.05	2	0.15±0.04	2	0.20±0.05
SiI	9	-0.15±0.05	9	0.02±0.07	4	-0.23±0.07	12	0.18±0.08	5	-0.48±0.07	9	-0.65±0.03	7	-0.25±0.04	9	0.06±0.06	8	-0.12±0.09	11	0.08±0.08
CaI	4	0.03±0.04	3	0.02±0.02	3	-0.13±0.06	3	0.11±0.04	2	-0.35±0.02	6	-0.72±0.04	3	-0.19±0.04	4	0.10±0.07	2	0.11±0.08	3	0.18±0.08
ScI	2	-0.01±0.10	2	0.14±0.08	1	-0.05	2	0.17±0.04	-	-	1	-1.73	1	-0.18	2	0.10±0.08	-	-	2	0.15±0.07
ScII	3	0.02±0.09	5	0.11±0.06	6	-0.14±0.05	5	0.11±0.06	5	-0.34±0.07	6	-0.96±0.05	7	-0.20±0.04	4	0.18±0.04	3	-0.04±0.07	7	0.15±0.06
TiI	21	-0.06±0.08	32	0.04±0.08	18	-0.23±0.07	26	0.00±0.05	16	-0.32±0.05	22	-0.79±0.05	22	-0.23±0.07	21	0.05±0.06	14	0.01±0.04	25	0.06±0.06
VI	18	-0.02±0.05	24	0.09±0.09	2	-0.24±0.01	19	0.14±0.07	3	-0.31±0.09	16	-0.99±0.06	7	-0.16±0.07	18	0.10±0.06	4	0.11±0.11	19	0.14±0.07
CrI	6	-0.24±0.07	6	-0.12±0.05	8	-0.38±0.06	12	0.12±0.07	7	-0.70±0.08	3	-1.17±0.03	6	-0.47±0.05	6	-0.21±0.07	4	-0.20±0.09	10	0.00±0.08
MnI	1	-0.25	1	-0.30	1	-0.69	1	-0.07	1	-0.91	2	-1.37±0.13	1	-0.82	-	-	1	-0.58	1	-0.10
FeI	71	-0.15±0.07	88	-0.09±0.07	64	-0.30±0.07	80	0.11±0.06	34	-0.55±0.08	55	-1.01±0.06	61	-0.43±0.06	73	-0.09±0.06	51	-0.13±0.06	77	0.05±0.06
FeII	5	-0.24±0.07	6	-0.14±0.07	4	-0.39±0.02	7	0.09±0.05	2	-0.68±0.06	6	-1.08±0.03	3	-0.46±0.02	5	-0.16±0.05	7	-0.25±0.08	7	0.01±0.08
CoI	5	-0.19±0.09	6	-0.07±0.10	3	-0.33±0.02	6	-0.02±0.14	4	-0.55±0.04	2	-1.02±0.07	4	-0.39±0.04	5	-0.05±0.07	5	-0.10±0.11	5	-0.03±0.07
NiI	21	-0.15±0.08	26	-0.04±0.06	20	-0.35±0.07	22	0.20±0.06	5	-0.60±0.04	15	-1.06±0.03	15	-0.42±0.06	25	-0.06±0.06	17	-0.19±0.06	26	0.04±0.07
YII	-	-	-	-	-	-	1	-0.08	2	-0.77±0.11	-	-	-	-	-	-	-	-	-	-
ZrII	-	-	-	-	1	-0.49	-	-	1	-0.41	1	-0.52	-	-	1	0.13	-	-	-	-
BaII	-	-	1	0.06	1	-0.22	1	0.03	1	-0.02	1	-0.41	1	-0.13	1	0.14	1	0.41	1	0.52
LaII	1	0.34	-	-	1	-0.32	-	-	-	-	1	-0.66	1	-0.40	-	-	1	0.06	2	0.15±0.09
NdII	1	0.02	1	0.01	1	-0.10	1	-0.13	2	-0.32±0.12	2	-0.78±0.09	2	-0.14±0.15	1	0.04	1	0.08	1	0.21
EuII	-	-	1	0.10	-	-	1	-0.04	1	-0.15	1	-0.77	1	-0.12	1	0.15	1	0.08	1	0.34

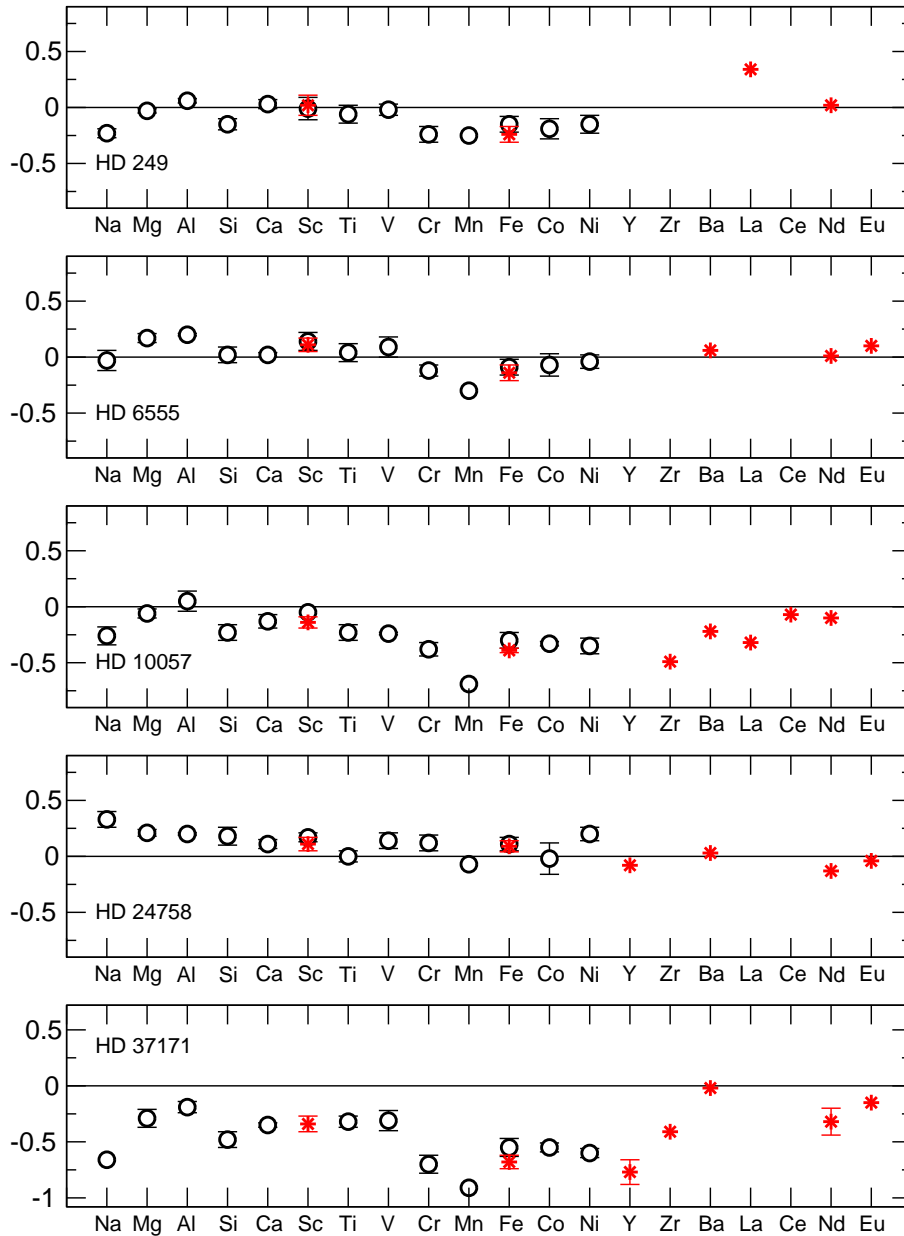


FIG. 1: Relative abundances of chemical elements in atmospheres of the studied stars. Abundances defined from neutral atoms marked by circles, from ions marked by asterisks.

LTE processes. According to [33, 35, 36], this doublet is formed deeper than other sodium lines, and the non-LTE processes do not introduce significant deviations in the abundance determination (<0.1 dex). Figure 2 presents the abundance trends for some elements with metallicity. The large circles mark our thick-disk red giants with their ordinal numbers from Table I. The small filled circles indicate the 74 thin-disk red giants from [4–7, 11, 15, 40–42] that we studied previously by a unified technique. The filled and open triangles indicate the thin-disk (29 stars) and thick-disk (22 stars) red giants from [3], who investigated the Galactic chemical evolution in the solar neighborhood. The solid and dashed lines indicate

the thin- and thick disk dwarfs from [8] averaged with a metallicity interval of 0.2 dex, while the shaded region denote a dispersion of 1σ .

DISCUSSION

Figure 2 demonstrates a compact arrangement of stars for all elements, except sodium, which reflects the evolution of elemental abundances in the Galaxy. The separation of the trends constructed for the thin and thick disks is characteristics of all elements, except sodium. Both dwarfs and giants of each of the disks

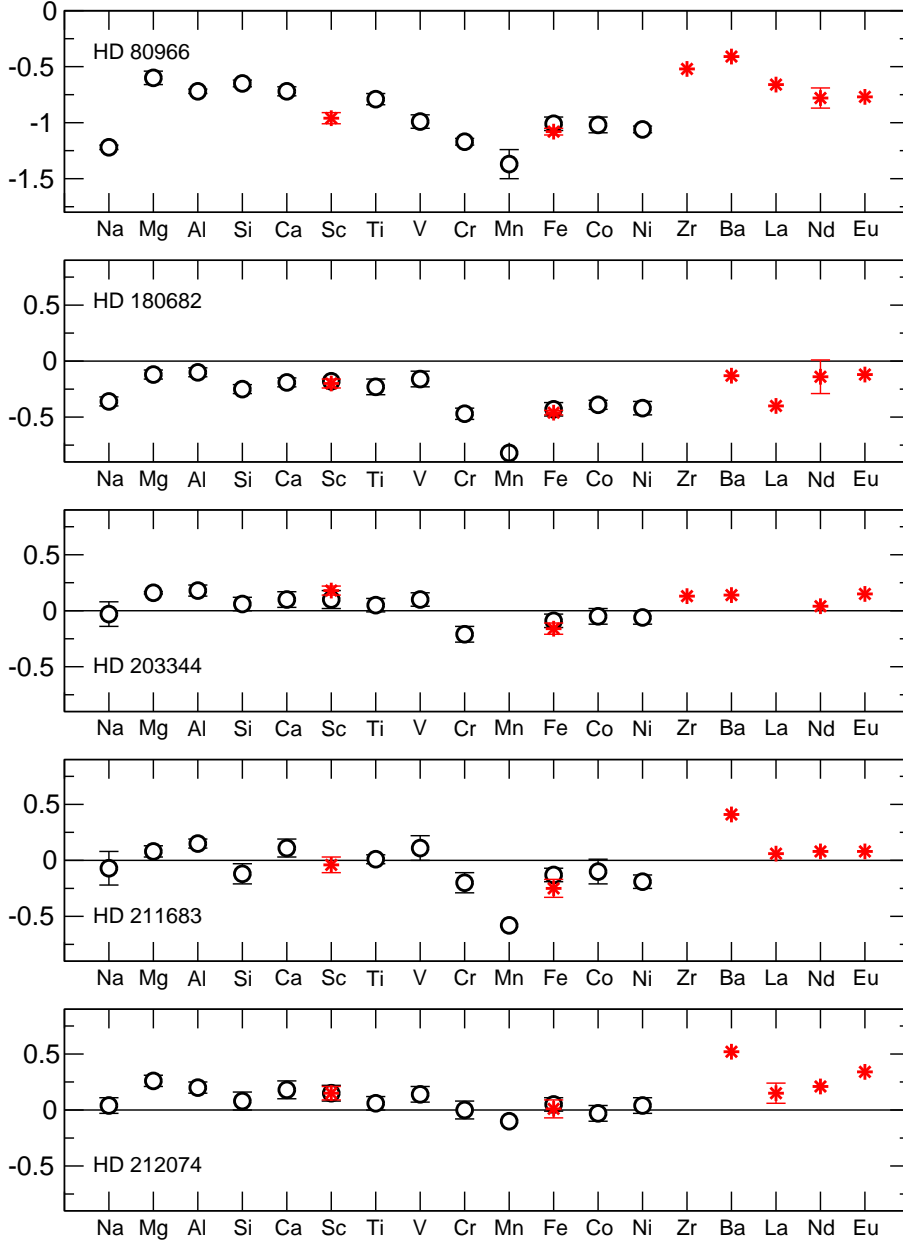


FIG. 1: continue

are located in the same regions, i.e., the abundances of these elements do not change over the elapsed lifetime of the star. In the case of sodium, a compact arrangement is observed only for dwarfs. The trends for thin- and thick-disk stars coincide, within the error limits. In contrast, red giants are chaotically scattered and no dependence on metallicity can be distinguished. Such a behavior suggests that the $[\text{Na}/\text{Fe}]$ abundance is determined not only by the chemical evolution of the Galaxy but also by the evolution of the star itself. The amount of sodium that was synthesized in the stellar core at the main-sequence stage and that was brought by convective flows into the stellar atmosphere is added to the initial

abundance. The thick disk red giants in Fig. 2, within the error limits, are located in the region of dwarfs and exhibit no detectable sodium overabundances. However, this is most likely the selection effect, because some of the thick-disk red giants from [3] and [39] have significant $[\text{Na}/\text{Fe}]$ overabundances. HD80966 with the lowest metallicity exhibits the lowest (and atypical of the remaining stars) abundance $[\text{Na}/\text{Fe}]=-0.21$ dex with an error of 0.02 dex calculated as the mean of the abundances from the two lines. Analysis of the possible errors by taking into account the uncertainty in the iron abundance and model parameters leads to a total error of about 0.12 dex. If we explain the low

TABLE V: Changes in abundances in atmosphere of the star HD37171 ($T_{\text{eff}}=4000\text{K}$ $\lg g=1.25$ $V_t=1.35 \text{ km s}^{-1}$) and HD212074 ($T_{\text{eff}}=4700\text{K}$ $\lg g=2.55$ $V_t=1.30 \text{ km s}^{-1}$) due changes in $\Delta T_{\text{eff}}=+100\text{K}$, $\Delta \lg g=+0.10$, $\Delta V_t=+0.10 \text{ km s}^{-1}$ and total error Δ

Element	N	$\Delta[E/H]_{HD37171}$				Δ	N	$\Delta[E/H]_{HD212074}$				Δ
		ΔT_{eff}	$\Delta \lg g$	ΔV_t	Δ			ΔT_{eff}	$\Delta \lg g$	ΔV_t	Δ	
NA1	1	0.10	0.00	-0.02	0.10		2	0.10	0.00	-0.02	0.10	
MG1	2	-0.02	0.02	-0.01	0.03		2	0.03	0.00	-0.03	0.04	
AL1	2	0.08	0.00	-0.03	0.09		2	0.08	0.00	-0.02	0.08	
SI1	5	-0.10	0.04	-0.01	0.11	11	-0.04	0.03	-0.01	0.05		
CA1	2	0.11	0.00	-0.03	0.11	3	0.08	-0.01	-0.02	0.08		
SC2	5	-0.03	0.04	-0.04	0.06	7	-0.02	0.04	-0.03	0.05		
TI1	16	0.14	0.01	-0.04	0.15	25	0.14	0.00	-0.03	0.14		
V1	3	0.14	0.01	-0.03	0.14	19	0.17	0.01	-0.05	0.18		
CR1	7	0.11	0.01	-0.04	0.12	10	0.10	0.00	-0.03	0.10		
MN1	1	0.03	0.02	-0.01	0.04	1	0.06	0.01	-0.01	0.06		
FE1	34	-0.02	0.03	-0.04	0.05	77	0.04	0.01	-0.04	0.06		
FE2	2	-0.21	0.08	-0.03	0.23	7	-0.11	0.06	-0.03	0.13		
CO1	4	-0.01	0.03	-0.05	0.06	7	0.06	0.02	-0.05	0.08		
NI1	5	-0.06	0.03	-0.04	0.08	26	0.01	0.02	-0.04	0.05		
Y2	2	-0.03	0.05	-0.01	0.06							
ZR2	1	-0.03	0.05	0.00	0.06	2	0.20	0.01	-0.01	0.20		
BA2	1	0.00	0.00	-0.13	0.13	1	0.02	0.02	-0.10	0.10		
ND2	2	0.04	0.04	-0.03	0.06	1	0.03	0.04	-0.02	0.05		
EU2	1	0.00	0.05	-0.02	0.05	1	-0.02	0.03	-0.05	0.06		

abundance by the error in determining the temperature, then it turns out that we underestimate the temperature approximately by 200 K. Such a change will lead to a significant discrepancy between the elemental abundances determined from lines with different lower level excitation potentials, while the position of the star on other plots in Fig. 2 will rise dramatically. The discrepancy will also affect the [FeI/H] and [FeII/H] abundances, which can be corrected by varying the surface gravity $\lg g$. However, the value of $\lg g$ determined here is in good agreement with $\lg g$ derived from the parallax (1.80 ± 0.15 and 1.86 ± 0.23 , respectively). Nevertheless, the thick-disk giants from our database, on average, exhibit a lower [Na/Fe] abundance than the thin-disk ones: 0.03 ± 0.10 and 0.17 ± 0.15 , respectively. [32], who investigated the chemical composition of red giants from two thick-disk open star clusters, NGC 2204 and NGC 2243, also pointed out that at a metallicity [Fe/H] from -0.4 to -0.2 and $\lg g$ from 1.5 to 2.9, the mean [Na/Fe] abundance is close to zero: 0.02 ± 0.04 . An increase in the atmospheric [Na/Fe] abundance of red giants is better demonstrated by Fig. 3, which shows the dependence on surface gravity $\lg g$. Both these quantities are determined directly from observations. In the figure, the thin-disk stars (filled circles) show a rise as the surface gravity decreases from $\lg g \approx 3-3.5$. The surface gravity is related to other fundamental stellar parameters by the relation $\lg g = -10.607 + \lg M/M_{\odot} + 4 \lg T_{\text{eff}} - \lg L$, where M/M_{\odot} is the stellar mass in solar masses and $\lg L$ is the stellar luminosity. At a constant

stellar mass, the decrease in $\lg g$ can be associated with a decrease in the effective temperature and an increase in the stellar luminosity. Such a behavior is typical of a star as it evolves along the red giant branch, and the appearance of sodium overabundances and the increase in sodium abundance due to the rise of sodium-enriched matter through convective flows [49] are associated precisely with this evolutionary stage. At this stage of stellar evolution, an enrichment of matter by sodium is possible only in the regions of nuclear reactions at the main-sequence phase. The hydrogen burning reaction in the neon-sodium cycle is the main source of sodium [17, 18]. In the interiors of low-mass (1-3 M_{\odot}) stars, this cycle is not closed and turns into the chain of reactions $^{20}\text{Ne}(p, \gamma)^{21}\text{Na}(\beta^+)^{21}\text{Ne}(p, \gamma)^{22}\text{Na}(\beta^+)^{22}\text{Ne}(p, \gamma)^{23}\text{Na}$. The first quantitative estimate of these reactions for supergiants is given in [23]: depending on the temperature, from 1/3 to 2/3 of the ^{23}Na nuclei pass into ^{20}Ne . At the same time, the sodium abundance in the atmospheres of F-K supergiants increases by a factor of 5 (0.7 dex), in agreement with the observational data and Fig. 3. Various conditions for the nuclear reactions of the neon-sodium cycle were also considered by [48] and [46].

The thick-disk red giants are marked in Fig. 3 by the large circles (from this paper, the ordinal numbers correspond to Table I) and squares (previously investigated ones). It can be seen from the figure that they are located systematically below the thin disk red giants, while for the region $\lg g < 2$ the separation between

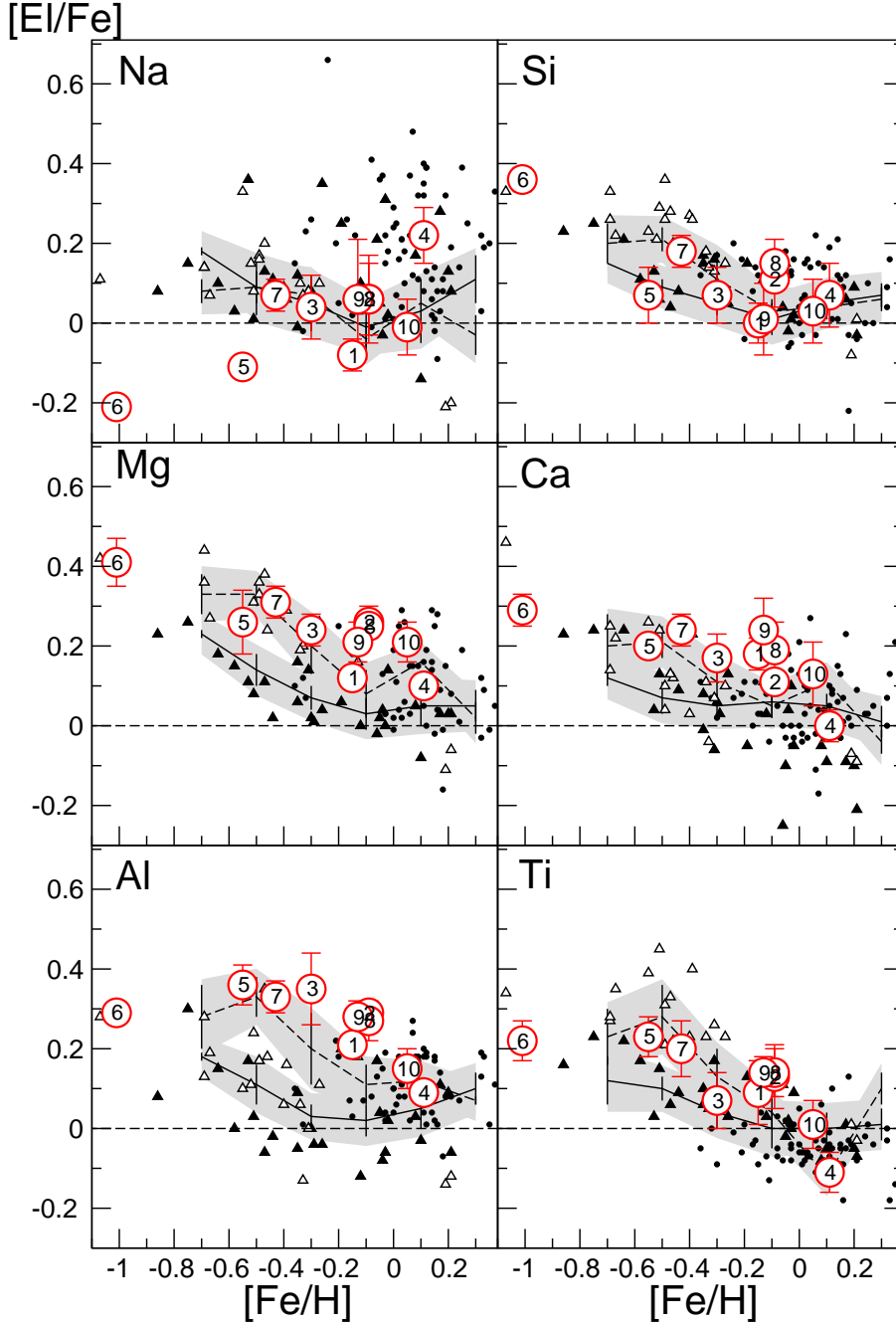


FIG. 2: Trends of abundances of $[\text{Na}, \text{Mg}, \text{Al}, \text{Si}, \text{Ca}, \text{Ti}/\text{Fe}]$ vs $[\text{Fe}/\text{H}]$ in atmospheres of the studied giants in comparison with data of other stars. Early studied red giants of thin disk marked by small filled circles. Filled and open triangles indicate on the reg giants from [3]. Continuous and dashed lines - the average data of dwarfs of thin and thick disk published by [8], with interval 0.2 dex in metallicity, filled area indicate 1σ dispersion level.

these two groups close in the number of stars exceeds the $[\text{Na}/\text{Fe}]$ abundance errors. Thus, the difference in $[\text{Na}/\text{Fe}]$ abundance in the atmospheres of thin- and thick-disk red giants is significant. Among the stars whose parameters were entered into the database, there are several pairs of thin- and thick-disk stars with similar parameters (T_{eff} , $\lg g$, $[\text{Fe}/\text{H}]$) (see [39]). Such stars also have similar masses and ages but differ only by the $[\text{Na}/\text{Fe}]$ abundance

and membership in different kinematic groups of stars in the Galaxy. Such a difference is not observed for the thin- and thick-disk dwarfs (see Fig. 2). Consequently, the initial sodium abundance must be also the same for those stars that have presently become red giants, while the nature of the difference is in the production of sodium in the NeNa cycle. A neon underabundance may exist in thick-disk objects. This is hard to check, because the

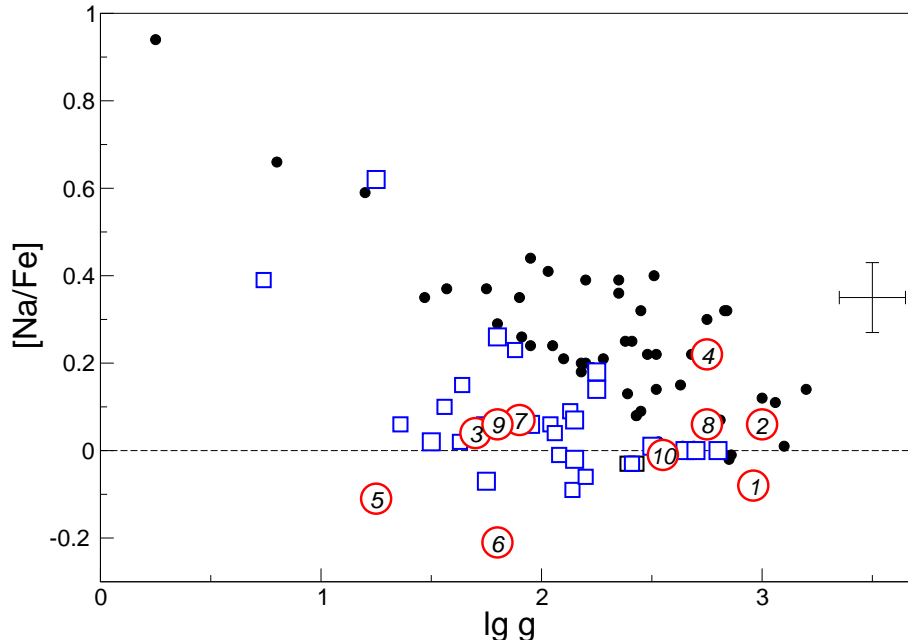


FIG. 3: $[\text{Na}/\text{Fe}]$ vs $\lg g$ in atmospheres of the studied giants of thin disk (filled circles) and thick disk (open rectangles) and red giants of current study (big open circles). The typical error bar in right part.

neon lines are difficult to observe. However, the main 20 Ne isotope is an α -process element, and its behavior with metallicity must follow the trends of other α -elements, i.e., an increase in abundance with decreasing metallicity [1]. In this case, we should have seen higher overabundances of sodium formed from neon in thick-disk giants, but the reverse is true. The ^{22}Ne underabundance is a possible cause. Indeed, [48] point out a significant reprocessing of ^{22}Ne into ^{23}Na , while the initial $^{22}\text{Ne}/^{23}\text{Na}$ abundance ratio in dwarfs is about 4.1. In any case, the difference between the atmospheric $[\text{Na}/\text{Fe}]$ abundances of thin- and thick disk red giants requires an explanation and invoking theoretical calculations.

CONCLUSIONS

Thus, based on spectroscopic observations, we determined the stellar atmosphere parameters for ten thick-

disk red giants. We confirmed the difference in atmospheric $[\text{Na}/\text{Fe}]$ abundance between thin- and thick-disk giants. Its nature may be related to the neon isotope abundance difference and this hypothesis requires verification.

Acknowledgments This work was supported by the Program for Support of Leading Scientific Schools (project 3602.2012.2), the “Nonstationary Phenomena in Objects of the Universe” Program of the Presidium of the Russian Academy of Sciences, and the Federal Agency for Science and Innovations (2012-1.5-12000-1011-014 “Influence of the Formation of Exoplanets on the Observed Properties of Outer Stellar Layers”)

-
- [1] Alibés, A., Labay, J., and Canal, R., *Astron. and Astrophys.* **370**, 1103 (2001), arXiv:astro-ph/0012505.
- [2] Allen, C. and Santillan, A., *Revista Mexicana de Astronomía y Astrofísica* **22**, 255 (1991).
- [3] Alves-Brito, A., Meléndez, J., Asplund, M., Ramírez, I., and Yong, D., *Astron. and Astrophys.* **513**, A35+ (2010), arXiv:1001.2521 [astro-ph.SR].
- [4] Antipova, L. I. and Boyarchuk, A. A., *Astronomy Reports* **45**, 700 (2001).
- [5] Antipova, L. I., Boyarchuk, A. A., Pakhomov, Y. V., and Panchuk, V. E., *Astronomy Reports* **47**, 648 (2003).
- [6] Antipova, L. I., Boyarchuk, A. A., Pakhomov, Y. V., and Panchuk, V. E., *Astronomy Reports* **48**, 597 (2004).
- [7] Antipova, L. I., Boyarchuk, A. A., Pakhomov, Y. V., and Yushkin, M. V., *Astronomy Reports* **49**, 535 (2005).
- [8] Bensby, T., Feltzing, S., Lundström, I., and Ilyin, I., *Astron. & Astrophys.* **433**, 185 (2005).
- [9] Bessell, M. S., Castelli, F., and Plez, B., *Astron. & As-*

- trophys. **333**, 231 (1998).
- [10] Boyarchuk, A. A., Antipova, L. I., Boyarchuk, M. E., and Savanov, I. S., *Astronomy Reports* **45**, 301 (2001).
- [11] Boyarchuk, A. A., Antipova, L. I., and Pakhomov, Y. V., *Astronomy Reports* **52**, 630 (2008).
- [12] Boyarchuk, A. A. and Boyarchuk, M. E., *Bulletin Crimean Astrophysical Observatory* **63**, 68 (1981).
- [13] Boyarchuk, A. A. and Lyubimkov, L. S., *Bulletin Crimean Astrophysical Observatory* **64**, 1 (1981).
- [14] Boyarchuk, A. A. and Lyubimkov, L. S., *Bulletin Crimean Astrophysical Observatory* **66**, 119 (1983).
- [15] Boyarchuk, A. A., Pakhomov, Y. V., Antipova, L. I., and Boyarchuk, M. E., *Astronomy Reports* **46**, 819 (2002).
- [16] Castelli, F. and Kurucz, R. L., in *Modelling of Stellar Atmospheres*, IAU Symposium, Vol. 210, edited by N. Piskunov, W. W. Weiss, and D. F. Gray (2003) pp. 20P+.
- [17] Cavallo, R. M., Sweigart, A. V., and Bell, R. A., *Astrophys. J.* **464**, L79+ (1996).
- [18] Cavallo, R. M., Sweigart, A. V., and Bell, R. A., *Astrophys. J.* **492**, 575 (1998).
- [19] Cayrel, G. and Cayrel, R., *Astrophys. J.* **137**, 431 (1963).
- [20] Cayrel de Strobel, G., Chauve-Godard, J., Hernandez, G., and Vaziaga, M. J., *Astron. & Astrophys.* **7**, 408 (1970).
- [21] Chen, B., Stoughton, C., Smith, J. A., Uomoto, A., Pier, J. R., Yanny, B., Ivezić, Ž., York, D. G., Anderson, J. E., Annis, J., Brinkmann, J., Csabai, I., Fukugita, M., Hindsley, R., Lupton, R., Munn, J. A., and the SDSS Collaboration., *Astrophys. J.* **553**, 184 (2001).
- [22] Denisenkov, P. A., *Soviet Astronomy Letters* **14**, 435 (1988).
- [23] Denisenkov, P. A. and Ivanov, V. V., *Soviet Astronomy Letters* **13**, 214 (1987).
- [24] Famaey, B., Jorissen, A., Luri, X., Mayor, M., Udry, S., Dejonghe, H., and Turon, C., *Astron. and Astrophys.* **430**, 165 (2005).
- [25] Gilmore, G. and Reid, N., *Monthly Notices Roy. Astron. Soc.* **202**, 1025 (1983).
- [26] Girardi, L., Bressan, A., Bertelli, G., and Chiosi, C., *Astron. & Astrophys. Suppl. Ser.* **141**, 371 (2000).
- [27] Greene, T. F., *Astron. Journal Supp.* **73**, 15 (1968).
- [28] Greenstein, J. L. and Keenan, P. C., *Astrophys. Journal* **127**, 172 (1958).
- [29] Helfer, H. L. and Wallerstein, G., *Astrophys. J. Supp.* **9**, 81 (1964).
- [30] Helfer, H. L. and Wallerstein, G., *Astrophys. J. Suppl.* **16**, 1 (1968).
- [31] Helfer, H. L., Wallerstein, G., and Greenstein, J. L., *Astrophys. J.* **129**, 700 (1959).
- [32] Jacobson, H. R., Friel, E. D., and Pilachowski, C. A., *Astron. Journal* **141**, 58 (2011).
- [33] Korotin, S. A. and Komarov, N. S., *Soviet Astronomy* **33**, 449 (1989).
- [34] Kurucz, R., “ATLAS9 Stellar Atmosphere Programs and 2 km/s grid. Kurucz CD-ROM No. 13. Cambridge, Mass.: Smithsonian Astrophysical Observatory, 1993.” (1993).
- [35] Lind, K., Asplund, M., Barklem, P. S., and Belyaev, A. K., *Astron. and Astrophys.* **528**, A103+ (2011), arXiv:1102.2160 [astro-ph.SR].
- [36] Mashonkina, L. I., Shimanskii, V. V., and Sakhbullin, N. A., *Astronomy Reports* **44**, 790 (2000).
- [37] Maurice, E., Andersen, J., Ardeberg, A., Bardin, C., Imbert, M., Lindgren, H., Martin, M., Mayor, M., Nordstrom, B., Prevot, L., Rebeiro, E., and Rousseau, J., *Astron. & Astrophys. Suppl. Ser.* **67**, 423 (1987).
- [38] Mishenina, T. V., Soubiran, C., Kovtyukh, V. V., and Korotin, S. A., *Astron. & Astrophys.* **418**, 551 (2004).
- [39] Pakhomov, Y. V., *Astronomy Letters* **38**, 101 (2012).
- [40] Pakhomov, Y. V., Antipova, L. I., and Boyarchuk, A. A., *Astronomy Reports* **55**, 256 (2011).
- [41] Pakhomov, Y. V., Antipova, L. I., Boyarchuk, A. A., Bizyaev, D. V., Zhao, G., and Liang, Y., *Astronomy Reports* **53**, 660 (2009).
- [42] Pakhomov, Y. V., Antipova, L. I., Boyarchuk, A. A., Zhao, G., and Liang, Y., *Astronomy Reports* **53**, 685 (2009).
- [43] Robin, A. C., Haywood, M., Creze, M., Ojha, D. K., and Bienayme, O., *Astron. & Astrophys.* **305**, 125 (1996).
- [44] Schopp, J. D., *Astron. Journal* **59**, 192 (1954).
- [45] Smiljanic, R., *Monthly Notices Roy. Astron. Soc.* **422**, 1562 (2012), arXiv:1202.2200 [astro-ph.SR].
- [46] Takeda, Y. and Takada-Hidai, M., *Pub. Astron. Soc. of Japan* **46**, 395 (1994).
- [47] van Leeuwen, F., *Astron. & Astrophys.* **474**, 653 (2007).
- [48] Wallerstein, G., Iben, I., Parker, P., Boesgaard, A. M., Hale, G. M., Champagne, A. E., Barnes, C. A., Käppeler, F., Smith, V. V., Hoffman, R. D., Timmes, F. X., Sneden, C., Boyd, R. N., Meyer, B. S., and Lambert, D. L., *Rev. Mod. Phys.* **69**, 995 (1997).
- [49] Weiss, A. and Charbonnel, C., *Mem del. Soc. Astron. Ital.* **75**, 347 (2004).